Chin. J. Astron. Astrophys. Vol. 6 (2006), No. 2, 210–216
(*http://www.chjaa.org*)

Chinese Journal of
Astronomy and
Astrophysics

Molecular Gas Distribution around the Supernova Remnant G40.5–0.5 *

Ji Yang[1,3], Jie-Long Zhang[2], Zhi-Yong Cai[1,3], Deng-Rong Lu[1,3] and You-Heng Tan[2]

[1] Purple Mountain Observatory, Chinese Academy of Sciences, Nanjing 210008;
jiyang@pmo.ac.cn
[2] Key Laboratory of Particle Astrophysics, Institute of High-Energy Physics, Chinese Academy of Sciences, Beijing 100049
[3] National Astronomical Observatories, Chinese Academy of Sciences, Beijing 100012

Received 2005 July 25; accepted 2005 December 4

Abstract The distribution of dense molecular gas around the supernova remnant G40.5–0.5 has been investigated by radio spectroscopic observations in the CO ($J = 1 - 0$) transition. The molecular gas is found to extend over the entire region of G40.5–0.5. A molecular shell, with a diameter of $\sim 26'$, coincides with the ionized gas as revealed by the cm-radio observations. This coincidence, along with the velocity discontinuity following the shell, provides direct evidence for interaction between the ionized gas and the dense molecular gas. No clear evidence for cosmic-ray acceleration can be identified from this SNR as previously suggested, due to positional uncertainty in relating the SNR shell defined by CO to the EGRET gamma-ray sources, GRO J1904+06, from the gamma-ray observations.

Key words: ISM: supernova remnant — ISM: clouds — radio lines: ISM— supernovae: individual (G40.5–0.5)

1 INTRODUCTION

A supernova (SN) explosion releases $\sim 10^{51}$ erg of kinetic energy into the interstellar medium (ISM). Among the progenitors of supernovae (SNe), the one responsible for a Type-II SN explosion is a disk population star with a mass $\geq 8\,M_{\odot}$ that was born inside dense molecular gas near the disk plane, completed its main-sequence evolution within 10^6 yr and now explodes as an SN. Due to their short lifetime, there remains sometimes plenty of dense molecular gas in their parental clouds (cf. Huang & Thaddeus 1986 for a survey). During the explosion, the expanding shell interacts with surrounding medium and transfers the kinetic energy of explosion into the ISM (Chevalier 1977), leaving behind a supernova remnant (SNR). For those type-I SNRs near the Galactic plane, it is expected that interactions with dense ISM may occur during their expansion. Particle accelerations via shocks between the SNR and ISM is believed to be responsible for the origin of high-energy cosmic rays, up to the extremely high energy regime of 100 TeV or above (for recent results, see, e.g., Tanimori et al.1998; Aharonian et al. 2001).

Since the discovery of interactions between SNR and dense molecular gas around IC 443 by Cornett et al. (1977) and DeNoyer (1979), numerous efforts have been made in observational

* Supported by the National Natural Science Foundation of China.

studies of such interactions, further combined with the origin of TeV cosmic ray particles (see the comprehensive summary by Torres et al. 2003). As a matter of fact, the evidence for interaction between SNR and dense gas is limited and the physical processes involved in the interaction and shock acceleration for cosmic ray origin is far from clear. One of the essential issues is to locate the exact site of TeV gamma-ray and to make clear identification between the nucleonic acceleration and shock motion in SNR.

The SNR G40.5–0.5 was first studied in detail at radio wavelengths by Downes et al. (1980, and the references therein). They found that the source shows a shell-like structure of non-thermal spectrum, with a spectral index $\alpha = 0.41$. The non-thermal spectrum was confirmed by the survey at 8.35 GHz (Langston et al. 2000). Sturner & Dermer (1995) proposed a possible identification of G40.5–0.5 with the EGRET gamma-ray source GRO J1904+06. Possible detection of TeV gamma-ray emission was suggested by Zhang et al. (2005) with the Tibet Air Shower Array.

In this study, we introduce observational studies of the dense molecular gas around the shell SNR and provide evidence for the interaction between the SNR and its neighboring dense ISM.

2 OBSERVATIONS

The observations were made in the ^{12}CO (J=1–0) line at 115.271 GHz using the 13.7 m millimeter-wave radio telescope of Purple Mountain Observatory at Delingha during 2003 January to May. The beam size was 60 arcsec and the main-beam efficiency, 42%. A 4-K cryogenic SIS receiver was installed on the telescope. The typical system temperature was around 250–300 K. The backend was an acousto-optical spectrometer (AOS) with a spectral coverage of 43 MHz, divided into 1024 channels. The spectral resolution is 75.7 kHz, equivalent to 0.2 km s^{-1} velocity resolution.

An on-off raster scan mapping was made over the source with a coverage of ΔR.A. = 72′ & ΔDecl. = 84′ centered at the source G040.59–0.48 at R.A.(J2000) = $19^{\rm h}07^{\rm m}11.9^{\rm s}$, Decl.(J2000) = 06°15′35″ given by Langston et al. (2000) and with a grid size of 2′ × 2′. For each point, a two minute on-source integration was adopted, resulting in a typical rms noise level of antenna temperature of 0.3 K. The data were reduced using the GILDAS/CLASS package developed by IRAM and the Observatoire de Grenoble.

3 RESULTS

CO emission was detected over most of the mapped area, as shown by the integrated intensity map in Figure 1. The molecular gas extends from the south-west (S-W) to the north-east (N-E), in general accordance with the local orientation of the Galactic plane. There is enhanced emission toward the north, and it is connected through an elongated structure to an extended cloud to the S-W.

3.1 The Velocity Structure of Molecular Gas

The emission of molecular gas extends over a radial velocity range of $V_{\rm LSR} = 0-90$ km s^{-1}. Figure 2 displays the velocity fields along two positional cuts, the left panel along the E-W direction and the right panel in the N-S direction. Three main velocity components can be separated. The first one is the foreground component at $V_{\rm LSR} = 5 - 40$ km s^{-1}, which is in fact composed of two separate velocity components originated from the local Lindblad ring and the local arm, respectively. The second component comes within $V_{\rm LSR} = 45-65$ km s^{-1} and the third is over $V_{\rm LSR} = 65-90$ km s^{-1}.

The locations of these components can be isolated in the channel maps. The first velocity component, $V_{\rm LSR} = 5 - 40$ km s^{-1}, is mainly located toward the northern part of the observed area, extended in accordance with the orientation of local galactic plane.

The channel map for the second component, $V_{\rm LSR} = 45 - 65$ km s^{-1}, shows a nearly circular enhancement of CO emission centered at the cm-continuum emission of G40.5–0.5 with a size of 26′, as shown in Figure 3. The shell is in good agreement with the radio continuum emission from Downes et al. (1980) and Langston (2000), as regards both the position and the angular size. Within the circular area there is little molecular gas, suggesting a shell structure. Along the shell CO emission is more prominent in the N-W sector, extended from a clump around (–20′, 0′). By

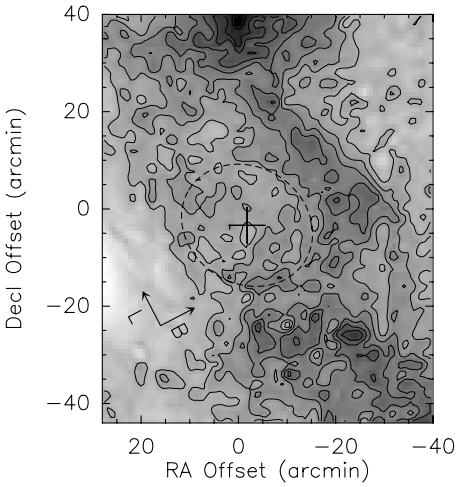

Fig. 1 Integrated intensity of CO line emission over the mapped area. The integration was made over the velocity range of $V_{\rm LSR} = 0 \sim 90$ km s^{-1}. Contour levels start from 62.7 K km s^{-1} by a step of 31.3 K km s^{-1}. The coordinates are offsets from R.A.(J2000) = $19^{\rm h}07^{\rm m}11.9^{\rm s}$, Decl.(J2000) = $06^\circ15'35''$. The position of SNR from cm-radio (Downes et al. 1980) is marked by a plus sign and its extent, traced by 120 mJy beam^{-1} in 2.7 GHz contour, is outlined by a dashed ellipse.

comparison of Figure 3 with the cm-radio distribution in Downes et al. (1980) and the Greenbank 4850 MHz survey (Condon et al. 1991), we find that the bright sector along the N-W of the shell agrees with the arc-like cm-radio enhancement.

By examining the position-velocity map back to Figure 2, it can be found that a velocity discontinuity corresponds well with the outer radius of the shell. The correspondence is especially clear along the E-W cut, where the discontinuity occurs at about $+10'$ E, and $-15'$ W. The good agreement in position and size between the molecular shell and the second component, $V_{\rm LSR} = 45 - 65$ km s^{-1}, and the corresponding velocity jump at the outer radius, provide direct evidence of a shock discontinuity between the SNR and its surrounding dense gas medium. The velocity range of the shock is about 10 km s^{-1}, which is quite close to the shock perturbed gas velocities found in IC 443 (DeNoyer 1977), 3C 391 (Reach & Rho 1999), and HB 21 (Koo et al. 2001).

3.2 The Shocked Molecular Emission

It has been shown that the shocked molecular emission is in agreement with the cm-radio emission. A swept-up shell is formed immediately outside of the ionized gas. From the enlarged map in Figure 3, the typical thickness of the swept-up shell, δr, can be estimated to be 2–4′, corresponding to 1.7–3.5 pc at the source's distance of 3.4 kpc (see Section 4.1). The mass of the shell is estimated to be $M = 2\pi r \delta r \times \sigma_{\rm gas}$, where $\sigma_{\rm gas}$ is the surface density, which is related to the column density of gas, $N({\rm H_2})$, by $\sigma_{\rm gas} = \mu m_{\rm H} N({\rm H_2})$, μ being the mean molecular weight taking helium into account. An average intensity of the ring surface, 27 K km s^{-1}, is reasonably estimated from Figure 3 and the CO intensity is converted to the column density of gas by $N({\rm H_2}) = 3.6 \times 10^{20} \int T_A^* dv$. Therefore, we have $N({\rm H_2}) = 9.7 \times 10^{21}$ cm^{-2} and $\sigma_{\rm gas} = 3.8 \times 10^{-2}$ g cm^{-2}. The mass of the swept-up gas within the shocked molecular shell is (3–6)$\times 10^4$ $M_\odot$. Assuming that the ambient gas was uniformly distributed before being swept-up into the shell by the SN explosion, we obtain an average number density of the initial molecular gas of (60–110) cm^{-3}.

It should be noted that the greatest uncertainty in the mass calculation comes from the conversion factor from CO intensity to molecular hydrogen column density. Bertsch et al. (1993) adopted a conversion factor of $(2 - 3) \times 10^{20}$, which differs from that given by Sanders et al. (1984) by

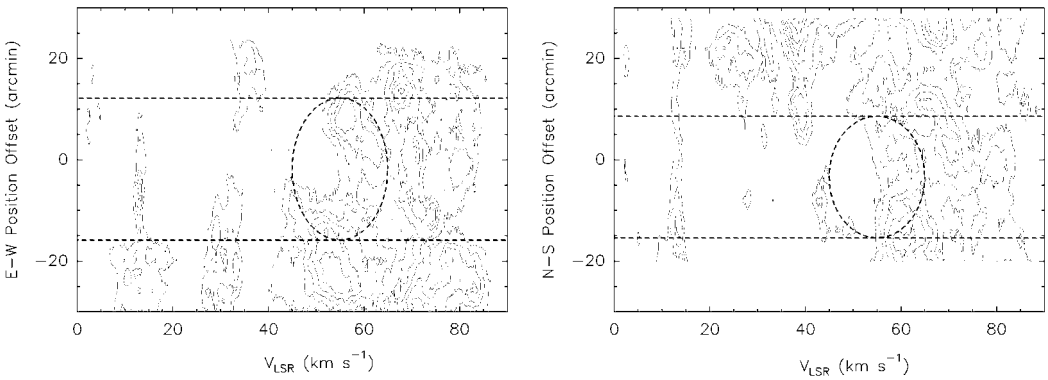

Fig. 2 Position-velocity diagram along the E-W cut (Left panel) and N-S cut (Right panel). Along each cut position, the spectra of vertical $\pm 4'$ positions and two velocity channels are binned, resulting in spatial resolution of $9'$ and velocity resolution of 0.2 km s^{-1}. Contour levels start from 1.0 K and increase at steps of 1.0 K. The dashed ellipses mark the extent of velocity discontinuity centered at $V_{\rm LSR} = 55$ km s^{-1}.

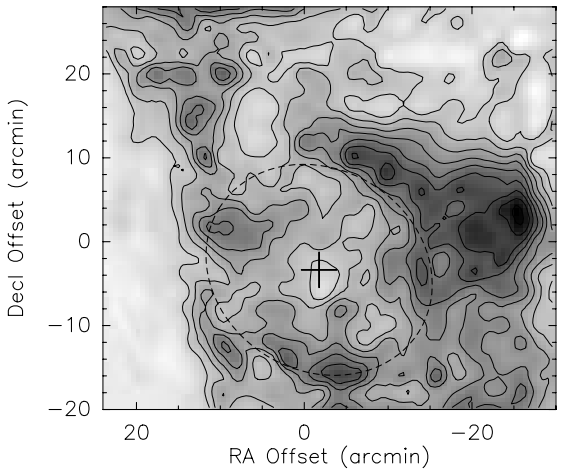

Fig. 3 Enlarged CO intensity map around G40.5–0.5. The line intensity was integrated over the velocity range of $V_{\rm LSR} = 45 \sim 65$ km s^{-1}. Contour levels start from 18.0 K km s^{-1} and increase by steps of 9.0 K km s^{-1}.

a factor of 1.2–1.8, while Dame et al. (2001) used another one of 1.5×10^{20}, which is a factor of 2 lower than that given by Sanders et al. (1984). Therefore, we expect that the calculated mass and other related quantities may have an uncertainty factor of 1.5–2.0.

The kinetic energy involved in the shocked gas is estimated to be $(3-6)\times10^{49}$ erg (see Table 1). This amount of kinetic energy is roughly 3%–6% of the total energy released during a supernova explosion. The estimated kinetic energy is comparable with that derived for 3C 391 (4×10^{49} erg) by Reach & Rho (1999) but is higher than the 6×10^{47} erg for IC 443 & 4×10^{48} erg for W44 (Seta et al. 1998), 3×10^{48} erg for W28 (Arikawa et al. 1999), 3×10^{47} erg for HB 21 (Koo et al. 2001) and 1×10^{48} erg for G347.3–0.5 (Fukui et al. 2003). Limited statistics shows that the large scatter in the kinetic energy deposit in the dense gas around SNRs is unlikely due to age difference, but rather, it is related to the total amount of gas going into the shocked region.

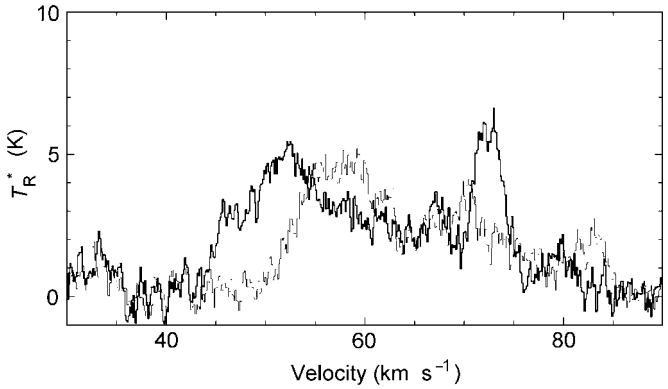

Fig. 4 Spectrum of shocked gas at selected positions. The thick line is for $(-14', -4')$ and the thin line is for $(+6', 0')$.

Table 1 Parameters of the Shocked Gas

Size of Shocked Shell	$28' \times 24'$ (=25 pc)
Gas Velocity	10 km s^{-1}
Shocked Mass	$(3-6) \times 10^4$ $M_\odot$
Momentum	$(3-6) \times 10^5$ $M_\odot$ km s^{-1}
Energy	$(3-6) \times 10^{49}$ erg

4 DISCUSSION

4.1 The Source Distance

The Σ-D relation is sometimes used to estimate the distance of the source (e.g., Case & Bhattacharya 1998; Arbutina et al. 2004). Taking into account the flux density at 8.35 GHz by Langston et al. (2000), the radio spectrum can be fitted by $\log F_\nu(\mathrm{Jy}) = 2.65 \pm 0.15 - (0.53 \pm 0.05) \log \nu$ (MHz), and the interpolated 1 GHz flux density is then 11.63 Jy.

We use the Σ-D relation by Huang & Thaddeus (1985), $\log \Sigma_{1\ \mathrm{GHz}} = -15.44 - 3.21 \log D(\mathrm{pc})$ and calculate the diameter of G40.5–0.5 to be 39.8 pc (here the surface brightness, $\Sigma_{1\ \mathrm{GHz}}$, is 2.59×10^{-21} W m^{-2} Hz^{-1} sr^{-1}). Using the angular diameter of $26'$ given by Downes et al. (1980) and Langston et al. (2000), the distance of the source is then estimated to be 5.3 kpc, almost identical to that given by Downes et al. (1980). The relation given by Arbutina et al. (2004) in fact gives a similar result. We should, however, be cautious here, because that the diameter estimated from the surface brightness is in fact close to the break point of the Σ-D curve commented by Guseinov et al. (2003), where a large error is possible in the estimation.

The line of sight to the source in the direction of galactic longitude $L = 40°$, intersects the nearside of the Sagittarius arm at ∼3 kpc, the far side at ∼9 kpc, and then the Perseus arm at ∼11.5 kpc, bringing quite a complexity into the source's distance. With the identified CO velocity components, $V_{\mathrm{LSR}} = 55$ km s^{-1}, and using the rotation curve of Clemens et al. (1988), we calculated the kinematic distance to be 3.4 kpc and a source diameter of 25 pc. In spite of the discrepancy in the derived distances by different methods, we shall adopt the source distance to be 3.4 kpc in this work.

The third component over $V_{\mathrm{LSR}} = 65 - 90$ km s^{-1} corresponding to the tangential velocity in the source galactic longitude is expected from the rotation curve to be at a distance of $\sim 6.5-7$ kpc. An examination of Figure 1 of Taylor & Cordes (1993) helps to find that this component is located

in the Scutum arm, hence the distance is 6.8 kpc. This component is not related to the $V_{\rm LSR}$ = 55 km s^{-1} component on the near side of Sagittarius arm.

4.2 Association of G40.5–0.5 with the High-Energy Sources

G40.5–0.5 is located within the coverage of Galactic Plane survey by Compton Gamma Ray Observatory. Near G40.5–0.5, the following gamma-ray sources have been reported: GRO J1904+06 (Fichtel et al. 1994), GeV J1907+0557 (Lamb & Macomb 1997), and 3EG J1903+0550 (Hartman et al. 1999). Sturner & Dermer (1995) suggested GRO J1904+06 is in association with G40.5–0.5. There is a local enhancement, AX J1907.4+0549, in the ASCA GIS image (Roberts et al. 2001). AX J1907.4+0549 is close to the 95% confidence contour level of the EGRET source GeV J1907+0557 and contains two weak point-line sources which, as mentioned by Roberts et al., may correspond to the bright spots from a single, extended source. Roberts et al. (2001) suggested that 3EG J1903+0550, but not GeV J1907+0557, is associated with G40.5–0.5 SNR. On the current CO map, either 3EG J1903+0550 or GeV J1907+0557 (AX J1907.4+0549) is located far to the southwest beyond the SNR defined by the range of the CO swept shell as well as in previous cm-radio maps. In particular, the relatively high position accuracy, $\sim 24''$, in the X-ray imaging (Roberts et al. 2001) helps to exclude any possibility of association, while the large positional uncertainty in the gamma-ray observation, typically $0.5^\circ - 1^\circ$, makes any such identification uncertain. Therefore, the possibility of their association with G40.5–0.5 is not verified and, for the case of G40.5–0.5, we did not find the evidence for nucleonic interaction similar to that found in RX J1713.7–3946 (Butt et al. 2001, 2002). In fact, previous identifications of the gamma-ray sources are somewhat confusing, partly due to positional ambiguities in the gamma-ray observations.

Deeper imaging in gamma-ray with higher position accuracy will be helpful to obtain the detailed spatial distribution of shocked materials, which will help to describe quantitatively the interaction between the SNR and the dense molecular medium in the direction of G40.5–0.5. Also, CO mapping extended toward GeV J1907+0557 (AX J1907.4+0549) will provide additional information in identifying the nature of this gamma-ray source.

5 CONCLUSIONS

Molecular-line emission in CO J=1–0 transition has been used to investigate the dense gas distribution around the SNR, G40.5–0.5. The following points may conclude this study:

(1) A large amount of ambient gas has been found around the object. Shock disturbed gas emission has been found from the SNR;
(2) The area of the shocked gas, with a size of $26'$ or 25 pc, is in general agreement with the ionized gas defined by cm-radio emission;
(3) The shocked gas velocity is of order 10 km s^{-1} and the kinematic energy involved in the gas is $(3-6)\times 10^{49}$ erg;
(4) The systematic velocity of the gas associated with the SNR is $V_{\rm LSR}$ = 55 km s^{-1}. G40.5–0.5 is located in the Perseus arm at distance 3.4 kpc and the possibility of previously suggested association with the gamma-ray source GRO J1904+06 is not clear.

Acknowledgements This work was funded by the National Natural Science Foundation of China (NSFC) through Grant 10133020. The authors acknowledge the staff members of Qinghai Radio Observing Station at Delingha for their supports in collecting the molecular line data. They also acknowledge the anonymous referee for valuable comments which helped to improve the manuscript.

References

Aharonian F., Akhperjanian A., Barrio J. et al., 2001, A&A, 370, 112
Arbutina B., Urošević D., Stanković M. et al., 2004, MNRAS, 350, 346
Bertsch D. L., Dame T. M., Fichtel C. E. et al., 1993, ApJ, 416, 587
Butt Y. M., Torres D. F., Combi J. A. et al., 2001, ApJ, 562, L167
Butt Y. M., Torres D. F., Romero G. E. et al., 2002, Nature, 418, 499
Case G. L., Bhattacharya D., 1998, ApJ, 504, 761
Chevalier R. A., 1977, ARA&A, 15, 175
Clemens D. P., Sanders D. B., Scoville N., 1988, ApJ, 327, 139
Condon J. J., Broderick J. J., Seielstad G. A., 1991, AJ, 102, 2041
Cornett R. H., Chin G., Knapp G. R., 1977, A&A, 54, 889
Dame T. M., Hartmann D., Thaddeus P., 2001, ApJ, 547, 792
DeNoyer L. K., 1979, ApJ, 232, L165
Downes A. J. B., Pauls T., Salter C. J., 1980, A&A, 92, 47
Fichtel C. E., Bertsch D. L., Chiang J. et al., 1994, A&AS, 94, 551
Fukui Y., Moriguchi Y., Tamura K. et al., 2003, PASJ, 55, L61
Guseinov O. H., Ankay A., Sezer A. et al., 2003, A&AT, 22, 273
Hartman R. C., Bertsch D. L., Bloom S. D. et al., 1999, ApJS, 123, 79
Huang Y.-L., Thaddeus P., 1985, ApJ, 295, L13
Huang Y.-L., Thaddeus P., 1986, ApJ, 309, 804
Koo B., Rho J., Reach W. et al., 2001, ApJ, 552, 175
Lamb R. C., Macom D. J., 1997, ApJ, 488, 872
Langston G., Minter A., D'Addario L. et al., 2000, AJ, 119, 2801
Reach W. T., Rho J., 1999, ApJ, 511, 836
Roberts M. S. E., Romani R. W. et al., 2001, ApJS, 133, 451
Sanders D. B., Solomon P. M., Scoville, N. Z., 1984, ApJ, 276, 182
Scoville N. Z., Yun M. S., Sanders D. B. et al., 1987, ApJS, 63, 821
Seta M., Hasegawa T., Dame T. M. et al., 1998, ApJ, 505, 286
Sturner S. J., Dermer C. D., 1995, A&A, 293, L17
Tanimori T., Hayami Y., Kamei S. et al., 1998, ApJ, 497, L25
Taylor J. H., Cordes J. M., 1993, ApJ, 411, 674
Torres D. F., Romero G. E., Dame T. M. et al., 2003, Phys. Rep., 382, 303
Zhang J., Tan Y., Lu H. et al., 2005, Chin. Phys. Lett., 22, 1560